JOURNAL OF MATERIALS SCIENCE 28 (1993) 561–568

Development of Al_2O_3 scale during oxidation of a wrought nickel-base alloy

H. M. TAWANCY
Materials Characterization Laboratory, Metrology, Standards and Materials Division, Research Institute, King Fahd University of Petroleum and Minerals, P.O. Box 1639, Dhahran 32161, Saudi Arabia

Oxidation exposures consisting of 1 min to 1000 h at 950–1150 °C in still air were used to study the development of surface scale on an Ni–16Cr–4.5Al–4Fe–0.04C–0.01Y alloy. Growth kinetics of the oxide scale were studied thermogravimetrically. Scanning electron microscopy and thin-foil analytical electron microscopy combined with energy dispersive X-ray spectroscopy as well as X-ray diffraction were used to characterize the morphology, structure and composition of oxide scale. After a primary stage of rapid kinetics, oxide growth followed a parabolic rate law with an activation energy of about 400 kJ mol^{-1}. During primary oxidation, the alloy developed an inner layer of $Ni(Al, Cr)_2O_4$ spinel and the outer scale contained discrete particles of NiO and Cr_2O_3. When steady-state conditions were established, the inner spinel was replaced by a yttrium-modified layer of α-Al_2O_3. Under steady-state conditions, oxide growth appeared to be controlled at least partially by outward diffusion of aluminium as indicated by the effect of exposure time on its concentration in the outer scale. Near the oxide–metal interface, yttrium was found to segregate to grain boundaries of α-Al_2O_3. Experimental results suggested that yttrium maintained a fine-grained structure of α-Al_2O_3 of improved elevated temperature mechanical strength.

1. Introduction

Many of the wrought nickel-, iron- and cobalt-base high-temperature alloys are environmentally protected by Cr_2O_3-base scale [1]. Protection by Cr_2O_3 at temperatures above about 1000 °C, however, is limited by its tendency to transform into volatile CrO_3 [2]. Accordingly, those alloys are not suitable for applications requiring extended exposure at temperatures in excess of 1000 °C. In contrast, Al_2O_3 is more protective at those temperatures because of its higher thermodynamic stability and slow growth rate [3]. However, the relatively high aluminium concentration needed to establish a continuous protective layer of Al_2O_3 resulting in poor fabricability, weldability and low-temperature ductility, limits the use of Al_2O_3-forming alloys to coatings and castings [4]. Such problems have been overcome to a great extent in the newly developed wrought, nickel-base Haynes* alloy 214 [5, 6]. Its nominal chemical composition is given in Table I. Above 1000 °C, alloy 214 derives its oxidation resistance from a thin tenacious layer of yttrium-modified Al_2O_3 [7]. It was the objective of this investigation to study the development of Al_2O_3 scale on alloy 214 during exposure in air at temperatures in the range 980–1150 °C.

TABLE I Chemical composition of alloy 214 (wt %)

	Nominal	Investigated
Ni	Bal.	Bal.
Cr	16	16.12
Al	4.5	4.37
Fe	4	2.65
Y	0.01	0.009
C	0.04	0.032
S	–	< 0.002

2. Experimental procedure

An alloy sheet of commercial grade was investigated. Its chemical composition is given in Table I. Specimens (25.4 m × 25.4 mm × 1.0 mm) were annealed in quartz capsules under an argon atmosphere ($\sim 10^{-4}$ torr; 1 torr = 133.322 pa) at 1095 °C as recommended by the manufacturer, and then water quenched. Subsequently, the specimens were ground to 120 grit finish and then ultrasonically cleaned in acetone. They were then exposed for 1 min to 1000 h at 980–1150 °C in still air using a resistance-heated furnace. A thermogravimetric unit was used to study the growth kinetics of the oxide scale. Scanning electron microscopy (SEM) and energy dispersive X-ray spectroscopy (EDXS) with a conventional beryllium-window detector were used to characterize the morphology and composition of surface scale. Structural analysis of the surface scale on oxidized specimens was carried out using X-ray diffraction (XRD). To examine oxidised specimens on the finer scale of transmission and scanning transmission electron microscopy (TEM/STEM) modes of an analytical electron microscope

* Haynes is a registered trademark of Haynes International Co.

(AEM), sheet specimens initially 1 mm thick were reduced to about 0.5 mm and then annealed as described above. Disc-shaped specimens, 3 mm diameter, were machined from the annealed specimens, ground to about 0.3 mm thick, metallographically polished, and then isothermally oxidized in air as described above. Oxidized specimens were polished on one side to prepare thin foils near the oxide–metal interface [8] in a solution consisting of 30% nitric acid in methanol at about $-20\,^{\circ}C$ until perforation occurred. Oxide films left behind were thinned in an ion-beam mill at 5 kV. All specimens were examined in an AEM operating at 200 kV and equipped with an ultra-thin window X-ray detector.

3. Results and discussion

3.1. Kinetics of oxidation

Overall oxidation of the alloy was found to follow parabolic kinetics. For example, Fig. 1 illustrates the specific weight gain as a function of exposure time at 1150 °C. Following an initial stage of primary oxidation, steady-state conditions were reached after about 1 h exposure or less. It is observed that the linear scaling rate was about 8.5×10^{-6} mg cm^{-2} h^{-1}. Also, there was no evidence for breakaway oxidation and the adherence of the scale was maintained after 1000 h exposure at 1150 °C. A similar result was reported under cyclic conditions [9]. From weight change measurements, the activation energy of the oxidation reaction was calculated to be about 400 kJ mol^{-1}, which is considerably smaller than the activation energy of aluminium lattice diffusion in Al_2O_3 ($\sim$500 kJ mol^{-1} [10]).

As illustrated later, steady-state scale growth appeared to be controlled by diffusional transport in a layer of yttrium-modified Al_2O_3. Most evidence points to the growth of Al_2O_3 scale being dominated by grain-boundary diffusion of oxygen [11–13]. Also, rare-earth elements such as yttrium may decelerate the kinetics of aluminium lattice diffusion [14–17]. However, it is also possible that both aluminium and oxygen diffusion contribute to scale growth [18]. Thus, the observed activation energy may reflect the contribution of both aluminium and oxygen diffusion to scale growth as further discussed later.

3.2. Primary oxidation

Secondary electron SEM images illustrating the development of surface scale on the same region of the alloy during primary oxidation at 1150 °C are shown in Fig. 2. Initially, the surface contained an aggregate of fine particles and an underlying scale. With continued exposure, the particles tended to agglomerate and increase in size. Fig. 3 illustrates an example of analysing the structure and composition of surface scale formed during primary oxidation. As can be seen, the scale consisted of an aggregate of NiO and α-Cr_2O_3, and an underlying spinel of the type Ni(Al, Cr)$_2O_4$. At this stage, very few particles of Al_2O_3 could be detected at the surface. Near the oxide–metal interface and parallel to the plane of oxidation, the scale consisted predominantly of Ni(Al, Cr)$_2O_4$ as illustrated in Fig. 4. Arcing of the diffraction rings in Fig. 4a suggested the presence of fibrous texture [19]. These observations appeared to be consistent with a generalized mechanism proposed to explain the oxidation behaviour of Ni–Cr–Al alloys [20, 21]. However, the spinel near the oxide–metal interface contained a greater concentration of aluminium (Fig. 4c) in comparison with the outer spinel (Fig. 3e). Possibly, this behaviour could be due to the relatively slow diffusivity of aluminium in the scale.

3.3. Steady-state oxidation

Under steady-state conditions, a larger proportion of α-Al_2O_3 particles were detected in the surface scale. Generally, however, these particles contained small concentrations of nickel, chromium and iron as illustrated in Fig. 5. Oxide growth appeared to be governed by lattice diffusion as was evident from its relatively flat faces [22]. With continued exposure within the steady-state stage, the extent of surface coverage by Al_2O_3 increased and NiO became enriched in chromium as demonstrated in Fig.6. Simultaneously, Cr_2O_3 almost completely disappeared, possibly by transforming into volatile CrO_3 and by incorporation of chromium in NiO and the spinel. During this stage, the scale near the oxide–metal interface was found to consist predominantly of Al_2O_3 as illustrated in the bright-field TEM image and the corresponding selected-area diffraction (SAD) pattern

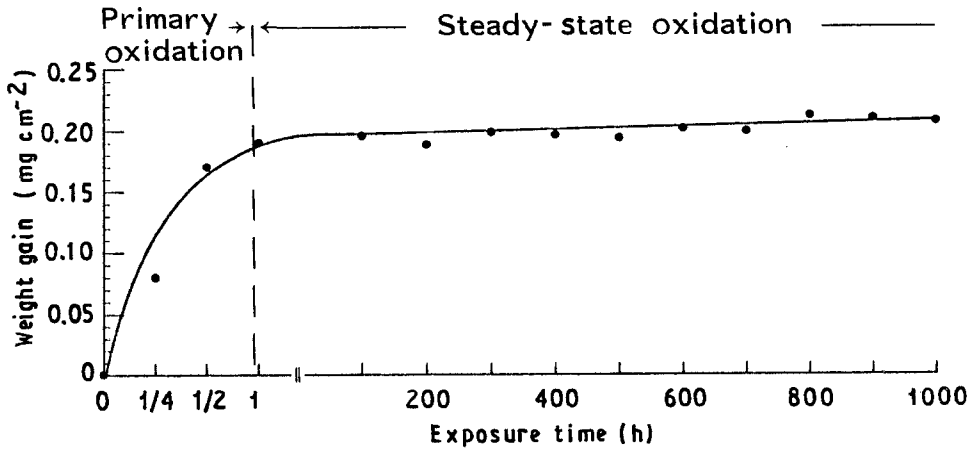

Figure 1 Effect of exposure time at 1150 °C on the specific weight gain.

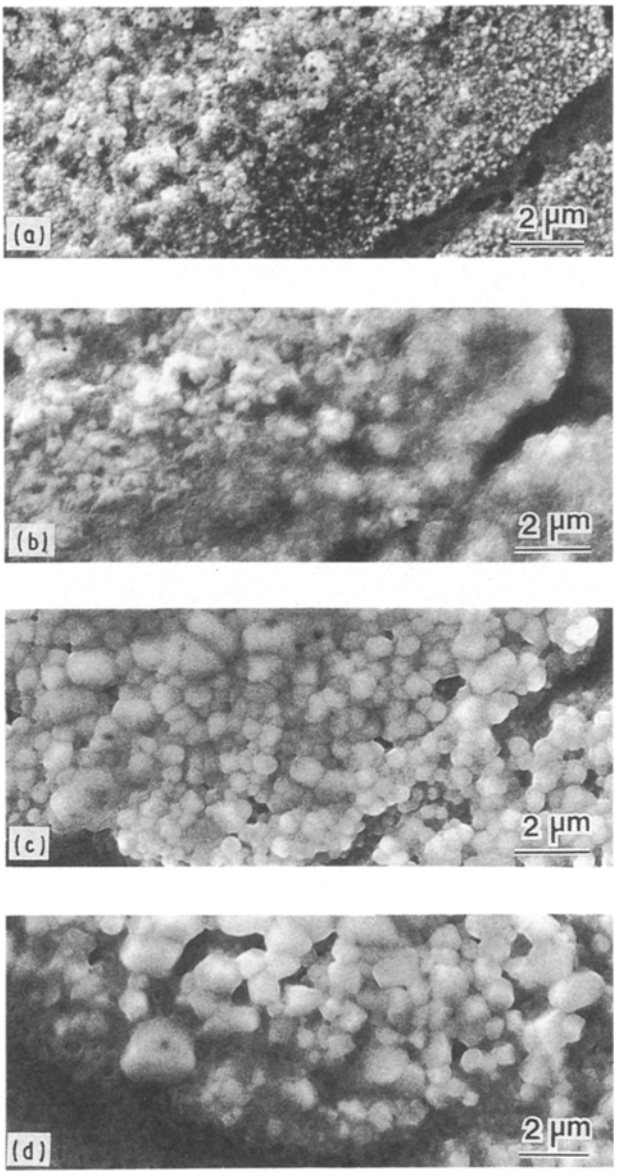

Figure 2 Secondary electron SEM images illustrating the evolution of surface scale on the same region during primary oxidation at 1150 °C. Time: (a) 1 min, (b) 5 min, (c) 15 min, (d) 1 h.

of Fig. 7a and b, respectively. It should be noted that characteristic reflections of α-Al_2O_3 such as $(1\,0\,\bar{1}\,4)$, $(1\,1\,\bar{2}\,0)$ and $(1\,1\,\bar{2}\,3)$ were absent in the selected-area diffraction (SAD) pattern of Fig. 7b suggesting the

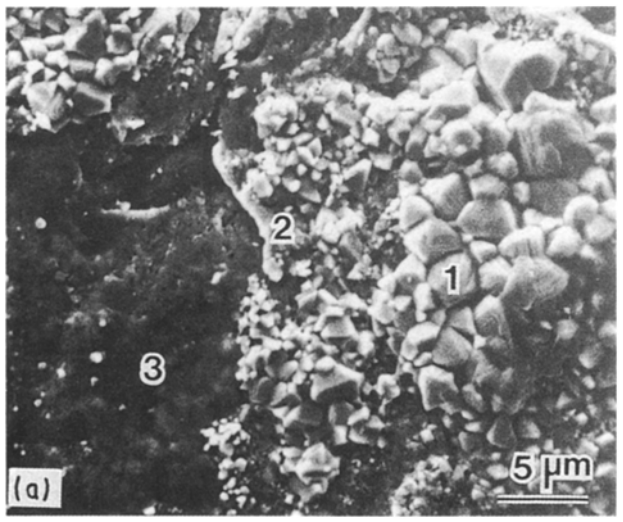

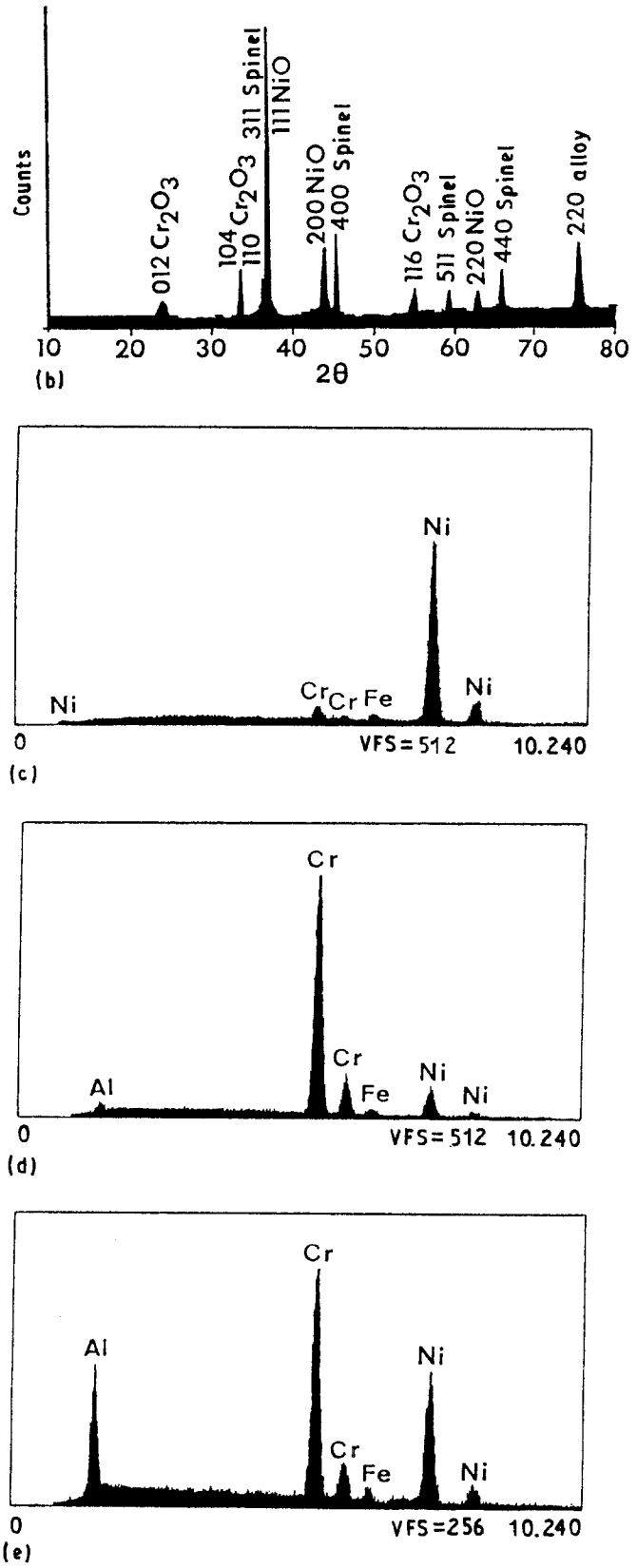

Figure 3 Analysis of the structure and composition of surface scale formed during primary oxidation (15 min exposure at 1150 °C). (a) Secondary electron SEM image illustrating the scale morphology. (b) Corresponding XRD pattern. (c) X-ray spectrum derived from Region 1 in (a). (d) X-ray spectrum derived from Region 2 in (a). (e) X-ray spectrum derived from Region 3 in (a).

presence of fibrous texture [19]. As shown in the X-ray spectrum of Fig. 7c, the oxide contained small amounts of chromium, nickel and yttrium. Considerable segregation of yttrium to grain boundaries of Al_2O_3 was observed as illustrated in the concentration

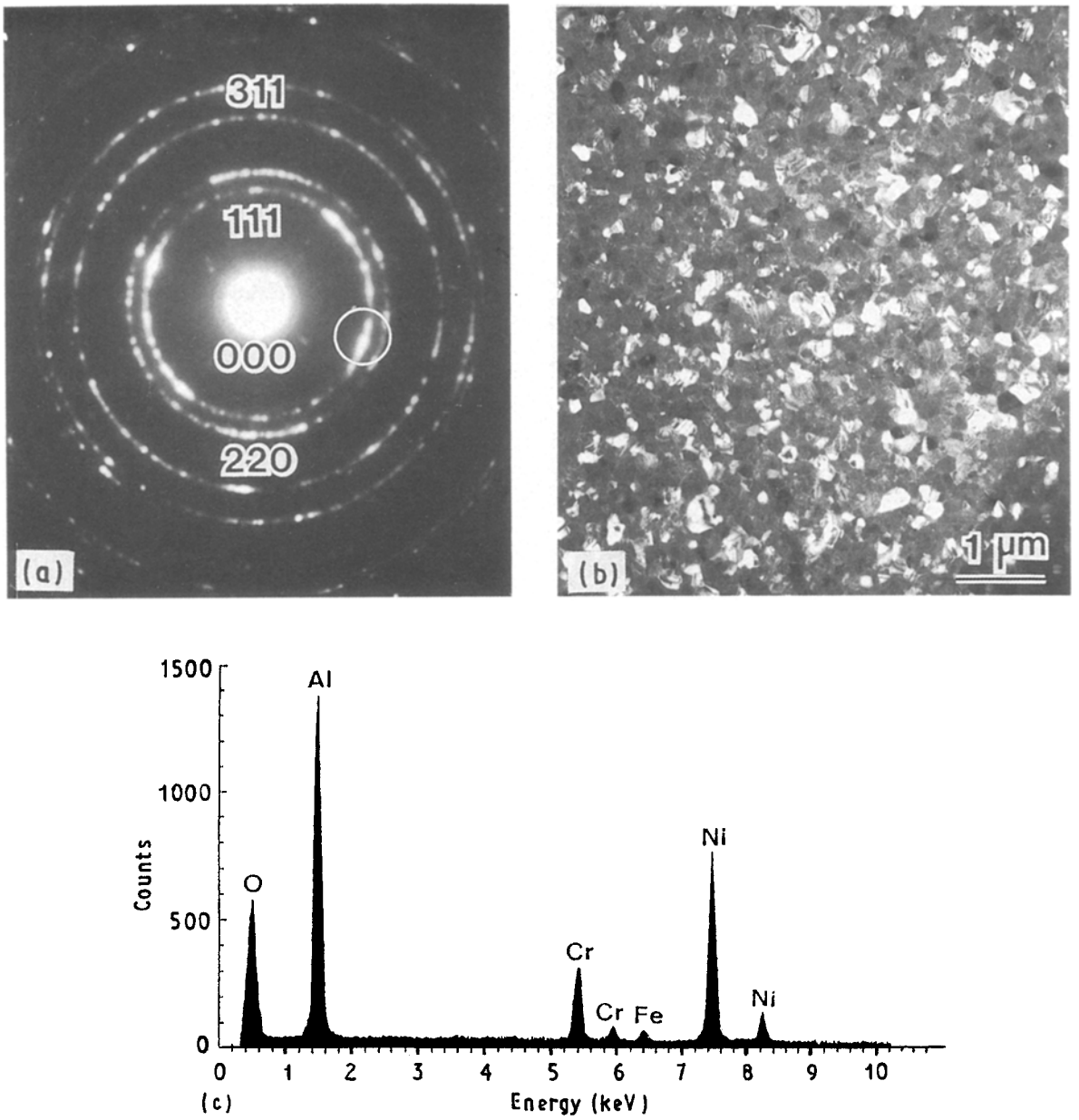

Figure 4 Analysis of the structure and composition of scale formed near the oxide–metal interface parallel to the plane of oxidation (15 min exposure at 1150 °C). (a) Selected-area diffraction pattern indexed in terms of the $NiAl_2O_4$ structure (cubic). (b) Corresponding dark-field TEM image formed with the encircled (1 1 1) reflection in (a). (c) X-ray spectrum derived in the STEM mode using a 20 nm probe diameter (point analysis).

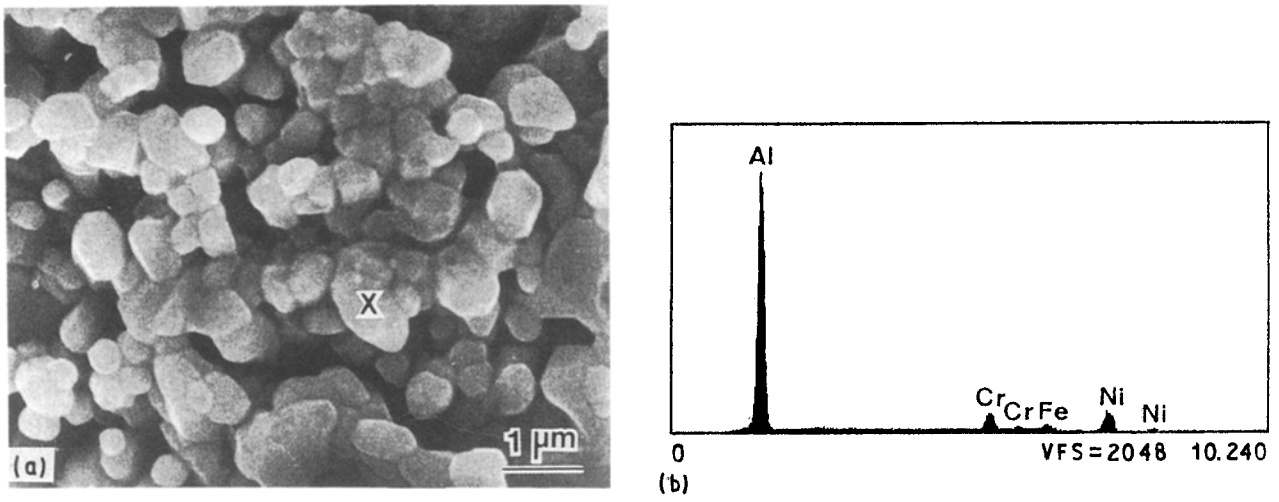

Figure 5 An example illustrating the presence of Al_2O_3 in the surface scale during steady-state oxidation (24 h exposure at 1150 °C). (a) Secondary electron SEM image illustrating particles of Al_2O_3. (b) X-ray spectrum derived from the particle marked (×) in (a).

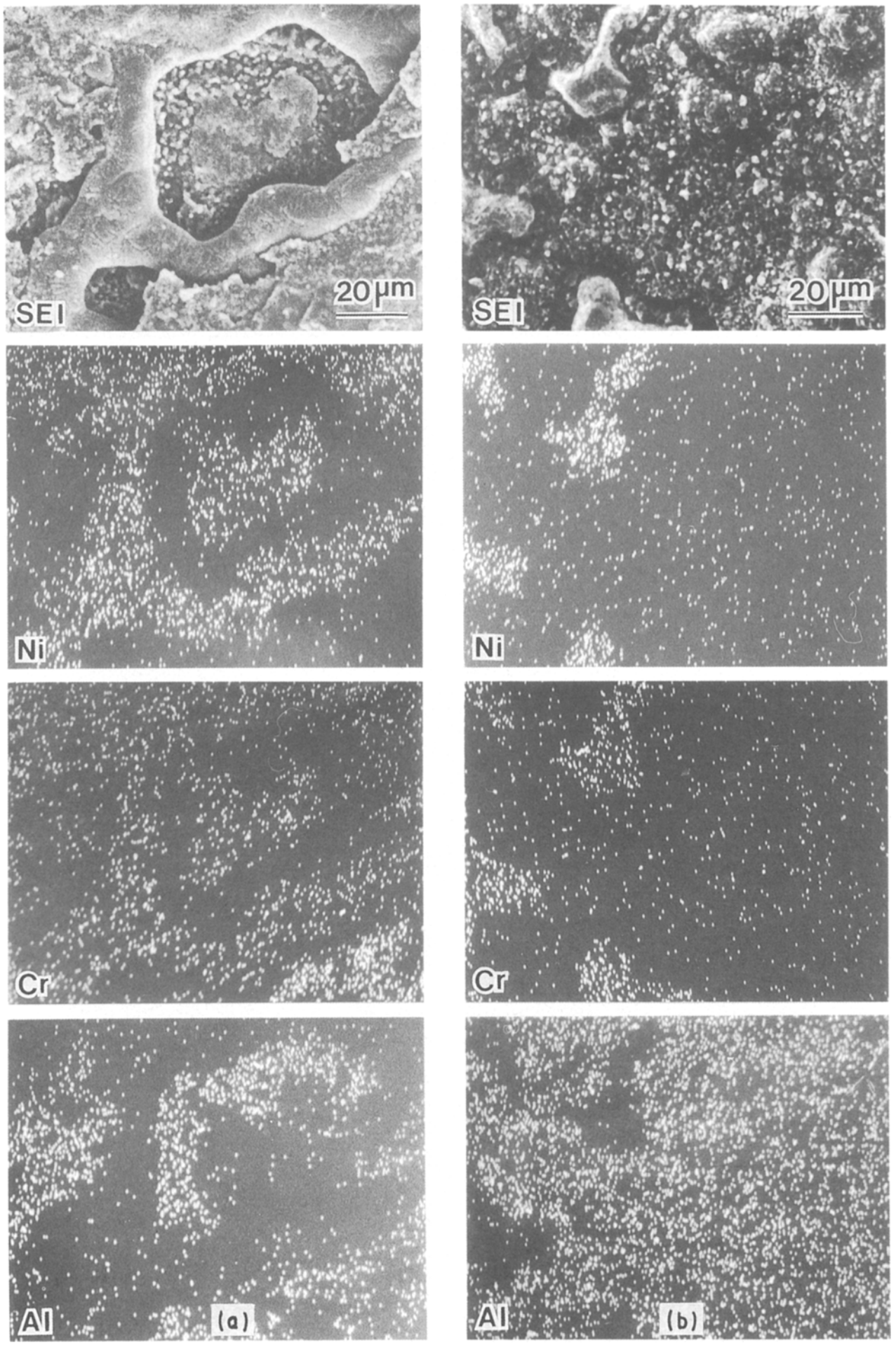

Figure 6 Secondary electron SEM images and corresponding X-ray mapping images of nickel, chromium and aluminium illustrating the effect of exposure time during steady-state oxidation on elemental distribution at the surface. (a) 100 h exposure at 1150 °C. (b) 1000 h exposure at 1150 °C.

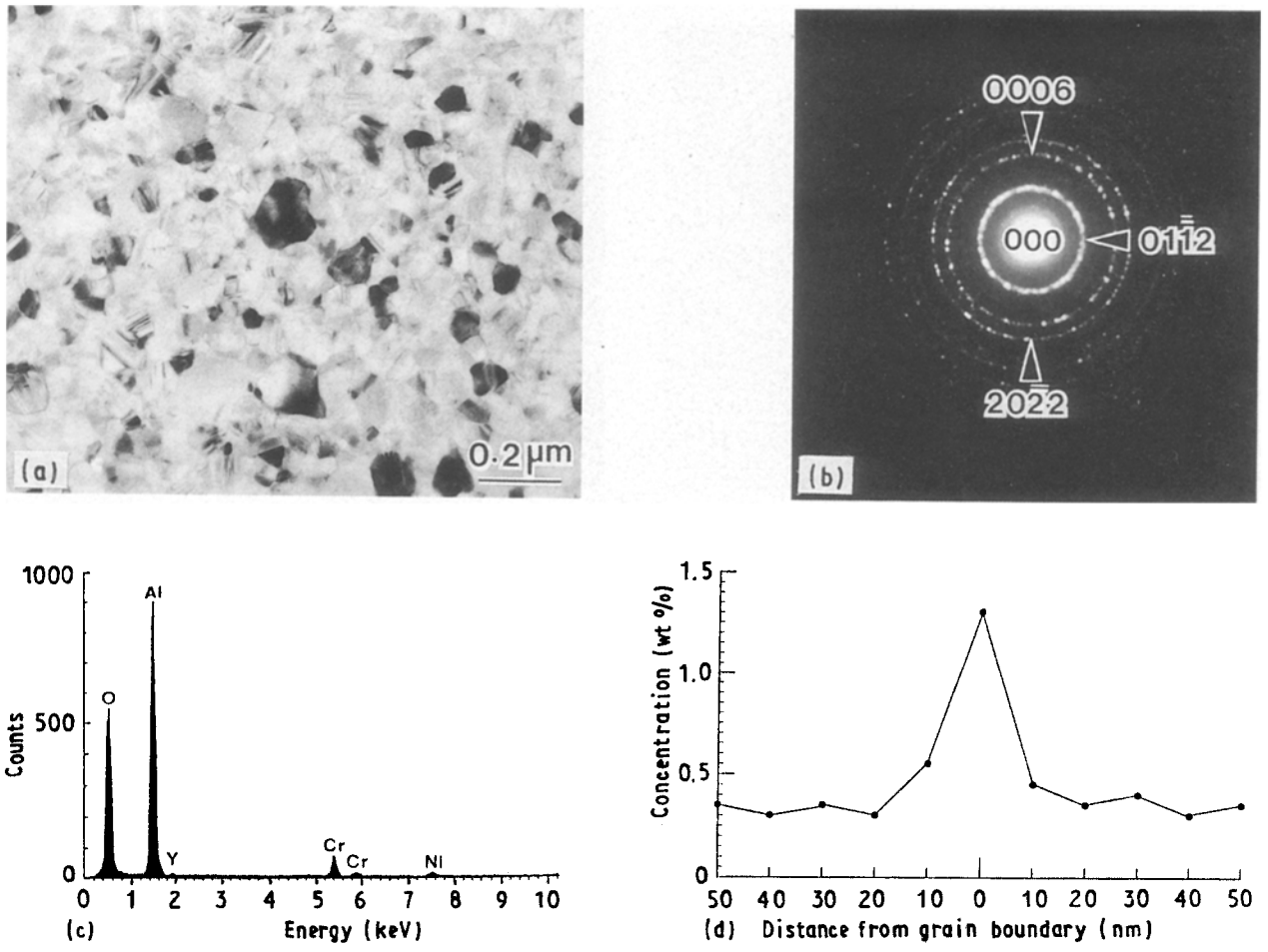

Figure 7 Analysis of the structure and composition of scale formed near the oxide–metal interface parallel to the plane of oxidation during steady-state oxidation (1000 h exposure at 1150 °C). (a) Bright-field TEM image. (b) Corresponding SAD pattern. (c) X-ray spectrum derived in the STEM mode using a 20 nm probe diameter. (d) Corresponding profile of yttrium across a grain boundary of Al_2O_3 (derived by point analysis in the STEM mode using a 2 nm probe diameter).

profile of Fig. 7d. Another distinctive feature of the Al_2O_3 scale near the oxide–metal interface was that its grain size remained virtually unchanged with exposure time as shown in the dark-field TEM images of Fig. 8, which could be related to yttrium segregation to grain boundaries. From these images, the grain size was estimated to be in the range 0.05–0.02 μm.

Although the beneficial effect of yttrium on the protective nature of Al_2O_3 is well recognized, a number of mechanisms, sometimes opposing, were sugges-

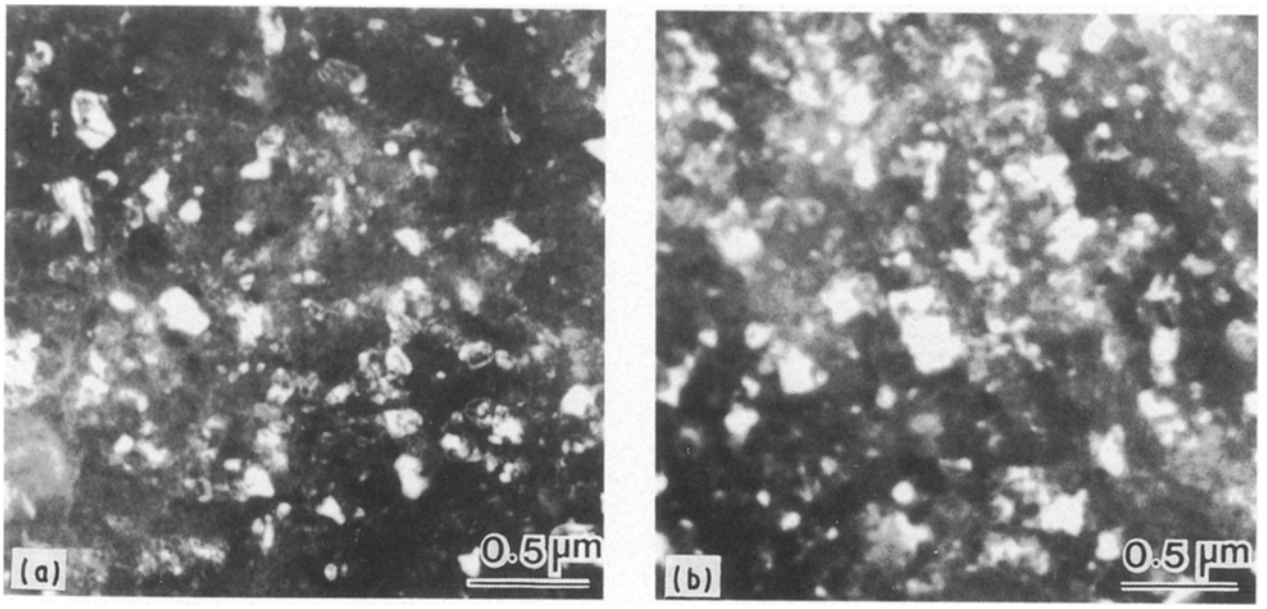

Figure 8 Dark-field TEM images formed with (0 1 1 2) reflection of Al_2O_3 to illustrate the effect of exposure time during steady-state oxidation on grain size near the oxide–metal interface. (a) 100 h exposure at 1150 °C. (b) 1000 h exposure at 1150 °C.

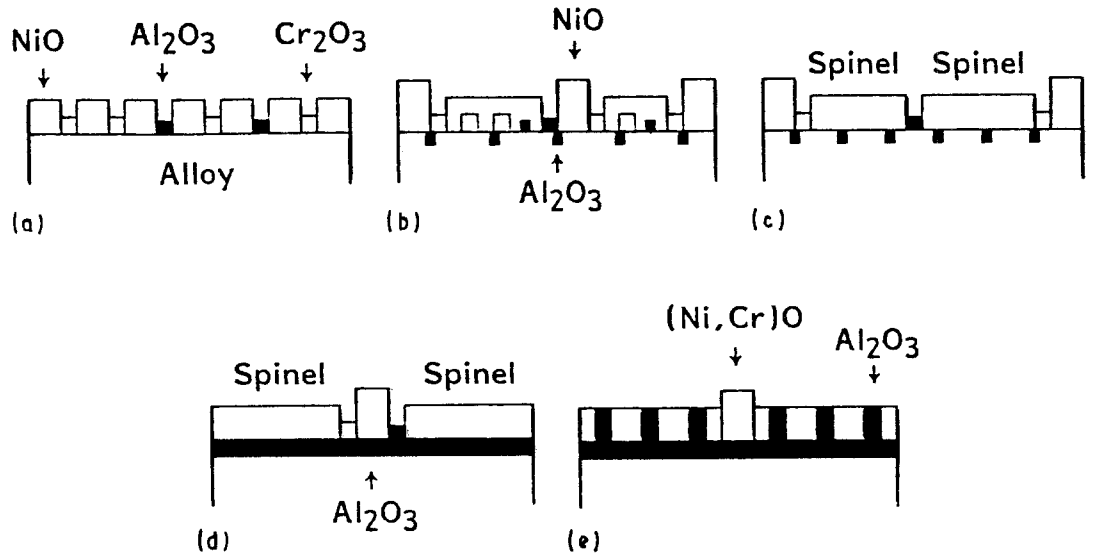

Figure 9 Schematic illustration of the development of Al_2O_3 scale. (a)–(c) Primary oxidation (d, e) steady-state oxidation.

ted to explain the yttrium effect [13, 18, 23–26]. However, the above results indicated that in the case of alloy 214, the beneficial effect of yttrium could be related to its segregation to grain boundaries of Al_2O_3. Among the beneficial effects of this segregation are maintaining a fine-grained structure with improved mechanical strength at elevated temperatures [12, 18, 23], and filling voids or pores along grain boundaries which improves its cohesion [27, 28]. Because grain boundaries act as effective sources of vacancies required for lattice diffusion [29], segregation of yttrium to grain boundaries would be expected to reduce the rate of vacancy generation which could decelerate the kinetics of aluminium diffusion and, in turn, the rate of scale growth.

3.3. Development of surface scale

Based upon the results presented earlier, the development of Al_2O_3 scale on alloy 214 could be envisioned as follows.

During the stage of primary oxidation (Fig. 1), oxides of nickel, chromium and aluminium were formed on the alloy surface in proportions determined by their concentration in the alloy [30] as schematically illustrated in Fig. 9a. However, as expected, NiO overgrew the slower growing Cr_2O_3 and Al_2O_3 and the three oxides combined to form a spinel of the type $Ni(Al, Cr)_2O_4$ as shown in Fig. 9b and c. Owing to the greater concentrations of nickel and chromium, some NiO and Cr_2O_3 remained on the surface (Fig. 9c). Because the oxygen activity established by these oxides was not sufficient to oxidize aluminium into Al_2O_3, oxygen diffused into the alloy and oxidized aluminium into Al_2O_3 [21, 22] as shown in Fig. 9b and c.

With continued exposure, a continuous layer of yttrium-modified Al_2O_3 in contact with the alloy was formed as observed and further growth of other oxides was blocked (Fig. 9d). At this stage, steady-state conditions were established and further oxide growth became controlled by diffusional transport in Al_2O_3. Subsequently, the extent of surface coverage by Al_2O_3 increased (Fig. 9e), which could be due to outward diffusion of aluminium. However, this could not exclude the possibility of inward diffusion of oxygen to oxidize aluminium at the spinel–Al_2O_3 interface [31]. Yttrium appeared to promote the formation of a thin tenacious layer of Al_2O_3 with improved mechanical strength.

4. Conclusion

During exposure for up to 1000 h at 950–1150 °C in still air, the oxidation kinetics of alloy 214 followed a parabolic rate law after an initial stage of primary oxidation. Initially, the alloy developed an inner layer of $Ni(Al, Cr)_2O_4$ spinel and the outer scale consisted of a mixture of NiO and Cr_2O_3. With continued exposure, steady-state conditions were established and the inner spinel was replaced by a yttrium-modified layer of α-Al_2O_3. At this stage, oxide growth appeared to be controlled at least partially by outward diffusion of aluminium with an activation energy of about 400 kJ mol^{-1}. Yttrium exhibited a preferential tendency for segregation to grain boundaries of α-Al_2O_3, which could maintain a fine-grained structure with improved mechanical strength at elevated temperatures.

Acknowledgement

The support of the Research Institute of King Fahd University of Petroleum and Minerals and its permission to publish this work are greatly appreciated. The material used in this investigation was kindly provided by the Haynes International Company.

References

1. J. L. SMIALEK and G. H. MEIER, in "Superalloys II", edited by C. T. Sims, N. S. Stoloff and W. C. Hagel (Wiley Interscience, New York, 1987) p. 293.
2. E. A. GULBRANSON and S. A. JANSSON, in "Heterogeneous Kinetics at Elevated Temperatures", edited by G. R. Belton and W. Worrell (Plenum Press, New York, 1970) p. 181.

3. A. KUMAR, M. NASRALLAH and D. L. DOUGLASS, *Oxid. Metals* **8** (1974) 227.
4. R. A. PERKINS, in "Proceedings of Conference on Corrosion/Erosion of Coal Conversion System Materials", edited by A. V. Levy (NACE, Houston, Texas, 1979) p. 351.
5. R. B. HERCHENROEDER, G. Y. LAI and K. V. RAO, *J. Metals* **35**(11) (1983) 16.
6. K. V. RAO and R. B. HERCHENROEDER, TMS Paper Selection (TMS-AIME, Warrendale, PA, 1984) Paper F84-10.
7. H. M. TAWANCY, *Met. Trans.* **22A** (1991) 1463.
8. PETER J. GOODHEW, "Specimen Preparation for Transmission Electron Microscopy of Materials" (Royal Microscopy Society, Oxford University Press, 1984) p. 36.
9. G. Y. LAI, *J. Metals* **37**(7) (1985) 14.
10. A. E. PALADINO and W. D. KINGREY, *J. Chem. Phys.* **37** (1962) 957.
11. F. H. STOTT, in "The Role of Active Elements in the Oxidation Behavior of High Temperature Metals and Alloys", edited by E. Lang (Elsevier Applied Science, London, New York, 1989) p. 3.
12. P. KOFSTAD, in "The Role of Active Elements in the Oxidation Behavior of High Temperature Metals and Alloys", edited by E. Lang (Elsevier Applied Science, London, New York, 1989) p. 367.
13. G. C. WOOD and F. H. STOTT, in "High Temperature Corrosion", edited by R. A. Rapp (NACE-6, Houston, Texas, 1983) p. 227.
14. T. A. RAMANARAYANAN, M. RAGHAVAN and R. PETKOVIC-LUTON, *J. Electrochem. Soc.* **131** (1984) 923.
15. *Idem, Oxid. Metals* **22**(3/4) (1984) 83.
16. K. P. REDDY, J. L. SMIALEK and A. R. COPPER, *ibid.* **17**(5/6) (1982) 429.
17. F. A. GOLIGHTLY, F. H. STOTT and G. C. WOOD, *ibid.* **10** (1976) 163.
18. H. HINDAM, and D. P. WHITTLE, *ibid.* **18** (5/6) (1982) 245.
19. P. HIRSCH, A. HOWIE, R. B. NICHOLSON, D. W. PASHLEY and M. J. WHELAN, "Electron Microscopy of Thin Crystals" (Krieger, Huntington, NY, 1977) p. 116.
20. F. S. PETTIT, C. S. GIGGINS, J. A. GOEBEL and E. J. FELTON, in "Alloys and Microstructural Design", edited by J. K. Tien and G. S. Ansell (Academic Press, New York, 1976) p. 349.
21. C. S. GIGGINS and F. S. PETTIT, *J. Electrochem. Soc.* **118** (1971) 1782.
22. G. M. RAYNAUD and R. A. RAPP, in "Microstructural Science: Corrosion, Microstructure and Metallography", Vol. 12, edited by D. O. Northwood, W. E. White and G. F. Vander Voort (ASM, Metals Park, OH, 1985) p. 197.
23. A. M. HUNTZ, in "The Role of Active Elements in the Oxidation Behavior of High Temperature Metals and Alloys", edited by E. Lang (Elsevier Applied Science, London, New York, 1989) p. 81.
24. *Idem, Mat. Sci. Eng* **87** (1987) 251.
25. F. H. STOTT and G. C. WOOD, **87** (1987) 267.
26. D. P. WHITTLE and J. STRINGER, *Phil. Trans. Roy. Soc. Lond., A* **295** (1980) 309.
27. J. JEDLINSKI, in "The Role of Active Elements in the Oxidation Behavior of High Temperature Metals and Alloys", edited by E. Lang (Elsevier Applied Science, London, New York, 1989) p. 131.
28. J. R. NICHOLLS and R. HANCOCK, *ibid.*, p. 195.
29. R. W. BALLUFFI, in "Grain-Boundary Structure and Kinetics" (ASM Materials Science Seminar, Metals Park, OH, 1980) p. 297.
30. G. C. WOOD, *Oxid. Metals* **2** (1970) 11.
31. J. E. HARRIS, *J. Metals* **39**(1) (1987) 34.

Received 23 September 1991
and accepted 4 May 1992